Instabilities in the Stratified, Wave-Forced Ocean Mixed Layer

Haney S.[1,2], B. Fox-Kemper[2,3], K. Julien[4]

[1]Department of Atmospheric and Oceanic Sciences, University of Colorado, Boulder, CO; [2]Cooperative Institute for Research in Environmental Sciences (CIRES), Boulder, CO; [3]Department of Geological Sciences, Brown University, Providence, RI; [4]Department of Applied Mathematics, University of Colorado, Boulder, CO.

Abstract

Instabilities in a stratified ocean mixed layer model with surface gravity wave forcing are examined to study the interactions between the surface gravity wave scale and the submesoscale. Linear instabilities at these two scales have been studied independently, however, this work serves to bridge the gap between these classes of instability. Wave effects are added to a linearized, stratified upper ocean model through the addition of Stokes-drift (a net current in the direction of wave propagation). In the limit of no wave forcing and strong stratification, this system is dominated by symmetric, geostrophic, or Kelvin-Helmholtz instability. In the limit strong wave forcing, the system is dominated by wave induced shear instability. The system is studied on a continuum between these two extremes to understand how the geostrophic and symmetric instabilities evolve as the wave forcing is increased. Initial results show that the wave induced modes become the gravest modes at modest wave forcing. The geostrophic mode is initially weakly amplified by the wave forcing, then at modest wave forcing appears to become a mixed mode. The symmetric mode is quickly damped as wave forcing is increased.

Scaling the Equations

The effect of the wave forcing is captured by considering the Boussinesq, wave-filtered, inviscid Craik-Leibovich Equations (Craik and Leibovich, 1976). Coriolis terms are included to include the effects of rotation under the f-plane approximation. The buoyancy is materially conserved, and advected by the Lagrangian (Eulerian and Stokes) flow.

$$\underbrace{\partial_t \mathbf{u}}_{\text{Acceleration}} + \underbrace{(\mathbf{u}\cdot\nabla)\mathbf{u}}_{\text{Advection}} - \underbrace{\mathbf{U}_s \times (\nabla\times\mathbf{u})}_{\text{Stokes Vortex}} + \underbrace{f\hat{\mathbf{k}}\times(\mathbf{u}+\mathbf{U}_s)}_{\text{Coriolis and Stokes Coriolis}} = \underbrace{-\nabla\pi}_{\text{Dynamic Pressure}} + \underbrace{b\hat{\mathbf{k}}}_{\text{Buoyancy}}$$

$$\partial_t \mathbf{u} + \left((\mathbf{u}+\mathbf{U}_s)\cdot\nabla\right) b = 0$$

$$\nabla\cdot\mathbf{u} = 0$$

$$W = 0 \ \text{ at } \ z = 0, -1$$

It is expected that there will be significant horizontal and time scale separation, thus motivating the horizontal variations to be non-dimensionalized by two different scales (l and L, with l ~ Ro L) with associated advective timescales (t and T). The wave field (thus Stokes drift) will be considered invariant horizontally, and in time. The dimensional variables are scaled as follows:

Non-dimensional numbers			
$Ro \equiv \frac{U}{fL}$	$Ri \equiv \frac{N^2H^2}{U^2}$	$\alpha \equiv \frac{H}{L}$	$\mu \equiv \frac{U_s(0)}{U}$
Dimensional Variable	**Scaling**	**Dimensional Variable**	**Scaling**
u, v	U	U_s, V_s	μU
w	$\frac{UH}{L}$	π	$U^2 max(Ro^{-1}, 1)$
b	$\frac{U^2}{H} max(Ro^{-1}, 1)$	b_z	N^2
$\partial_x,\ \partial_y$	$\frac{1}{L}\partial_x = \frac{1}{L}\partial_X,\ \frac{1}{L}\partial_y = \frac{1}{L}\partial_Y$	∂_z	$\frac{1}{H}\partial_z$

The Background Flow

Assuming these scalings, the flow is decomposed into average and perturbation terms. The averaged terms represent the large scale background flow, with the small horizontal space and fast time scales (x,y,t) averaged over. u', v',w' ~ O(Ro) and b', π' ~ O(Ro^2). The buoyancy and pressure scale with Ro^2 so that the small scale pressure perturbations scale with u'^{2}, unlike the large scale pressure which is scaled in expectation of near thermal wind balance. Averaging the equations over the small scales and assuming Ro << 1 gives the O(1) background flow.

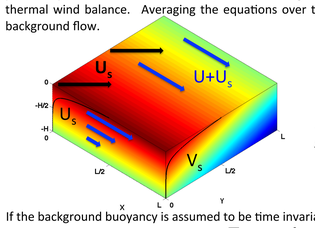

$$\bar{\Pi}_X - (\bar{V} + \mu V_s) = 0$$

$$\bar{\Pi}_Y + (\bar{U} + \mu U_s) = 0$$

$$\bar{\Pi}_z - \bar{B} = 0$$

$$\bar{B}_T + \left(\bar{U} + \mu U_s\right)\bar{B}_X + \left(\bar{V} + \mu V_s\right)\bar{B}_Y = 0$$

$$\bar{U}_X + \bar{V}_Y = 0$$

If the background buoyancy is assumed to be time invariant, and an initial condition on buoyancy is

$$\bar{B}\,|_0 = M^2 Y + N^2 z$$

where M^2 and N^2 are constants, then the flow is in hydrostatic, geostrophic balance with the Lagrangian velocity, or "Lagrangian Thermal Wind Balance." Therefore, the Lagrangian background flow is unaffected by the presence of Stokes drift. Despite this, it will be shown that the same is not true of the perturbed flow. The Stokes drift is chosen to be exponentially decaying with depth, with a decay scale chosen here to be H/10, consistent with observations.

The Perturbed Flow

Subtracting the balanced background flow from the full equation set gives the perturbation equations. Assuming α^2 << Ro, and posing a normal mode anzatz,

$$u'(x,y,z,t) = \tilde{u}(z) e^{i(kx+ly+\sigma t)}$$

and similarly for v', w', b', and π', the perturbation equations become,

$$\left(i\sigma + ik\bar{U}\right)\tilde{u} - \left(ik\mu V_s + 1\right)\tilde{v} + \bar{U}_z\tilde{w} + ik\tilde{\pi} = 0$$

$$\left(1 - il\mu U_s\right)\tilde{u} + \left[i\sigma + ik\left(\bar{U} + \mu U_s\right) + il\bar{V}\right]\tilde{v} + \bar{V}_z\tilde{w} + il\tilde{\pi} = 0$$

$$-\mu U_s\tilde{u}_z - \mu V_s\tilde{v}_z + \frac{\alpha}{Ro}\left[i\sigma + ik\left(\bar{U} + \mu U_s\right)\right]\tilde{w} - \tilde{b} + \tilde{\pi}_z = 0$$

$$-\tilde{v} + Ri\tilde{w} + \left[i\sigma + ik\left(\bar{U} + \mu U_s\right)\right]\tilde{b} = 0$$

$$ik\tilde{u} + il\tilde{v} + \tilde{w}_z = 0$$

In the case of no wave forcing (μ = 0) the background and perturbation equations are identically the baroclinic, non-hydrostatic equation set described by Stone (1971).

Growth Rates

The perturbation equations are solved numerically using Chebyshev spectral modes. Figure 1 shows the growth rates (σ) for Ri = 0.9, α = 0.006, Ro = 0.01, and various values of μ at various horizontal wavenumbers k and l. Ri = 0.9 is chosen so that both geostrophic and symmetric modes exist in comparable magnitude when there is no wave forcing (upper left panel of figure 1).

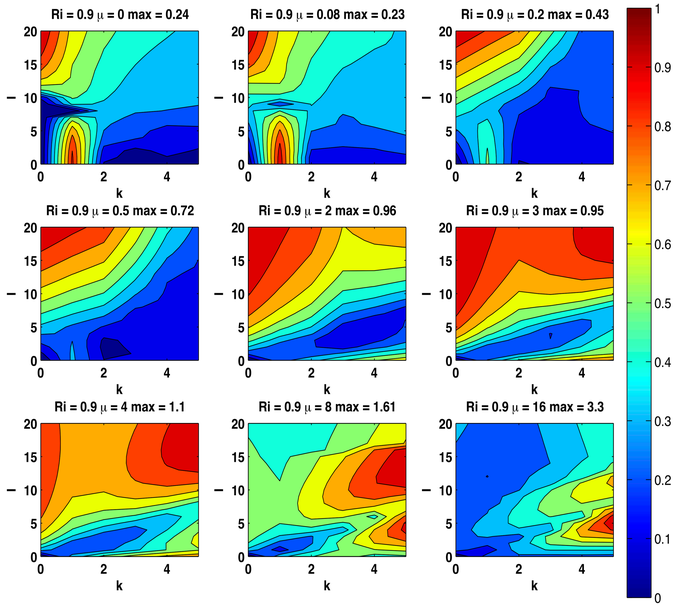

Figure 1. Maximum growth rate Im(σ) for Ri = 0.9, α = 0.006, Ro = 0.01, θ = π/4, and the indicated μ. Each panel is normalized to the maximum growth rate for that value of μ.

As the wave forcing increases the geostrophic and symmetric modes are overshadowed by instabilities at high wavenumber. This is unlike the transition to Kelvin Helmholtz instability in that increasing Ri without Stokes drift results in a stronger symmetric instability (high l, low k). The Stokes drift does increase the Eulerian Ri, however the Lagrangian Ri (which is listed) is unchanged in the presence of Stokes drift. Therefore, the high wavenumber instabilities shown are expected to be due to the Stokes vortex terms in the perturbation equations.

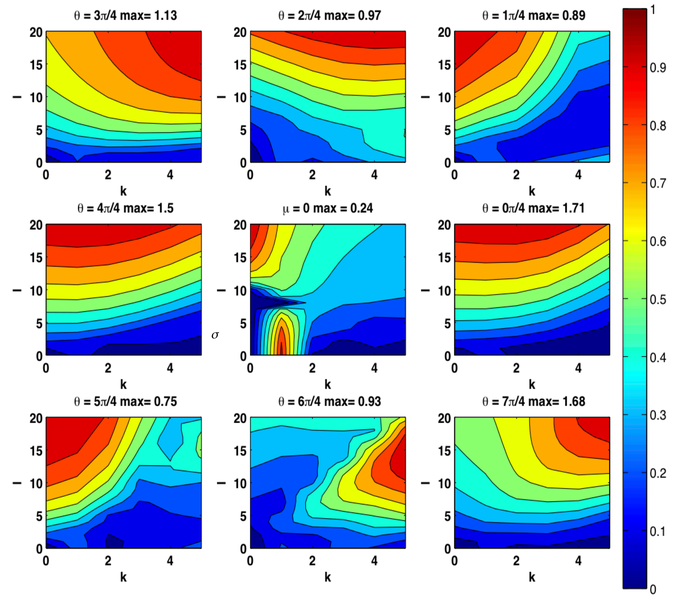

Figure 2. Maximum growth rate Im(σ) for Ri = 0.9, α = 0.006, Ro = 0.01, μ = 1, and the indicated θ. Each panel is normalized to the maximum growth rate for that value of θ. The location of the panels corresponds to the direction of the Stokes drift θ (e.g. θ = π/4 is the upper right panel).

Vertical Structure

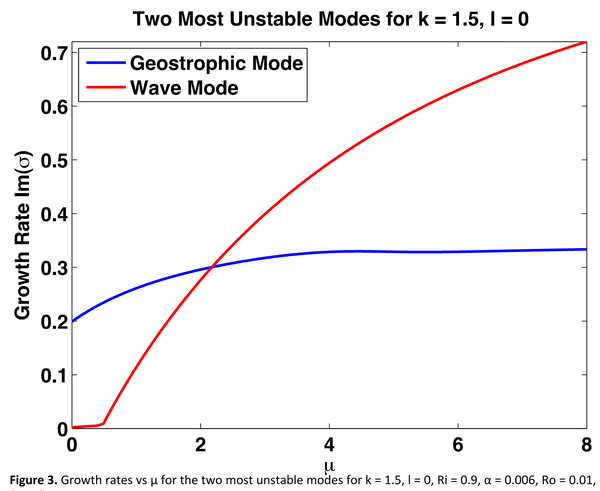

Figure 3. Growth rates vs μ for the two most unstable modes for k = 1.5, l = 0, Ri = 0.9, α = 0.006, Ro = 0.01, θ = π/4.

Fig. 1 shows that the most unstable mode quickly becomes high wavenumber as wave forcing is increased, however, it is clear from fig. 3 that this does not mean that the geostrophic mode is gone, but rather sub-dominant. It is also clear that the geostrophic mode is weakly modulated by the wave forcing.

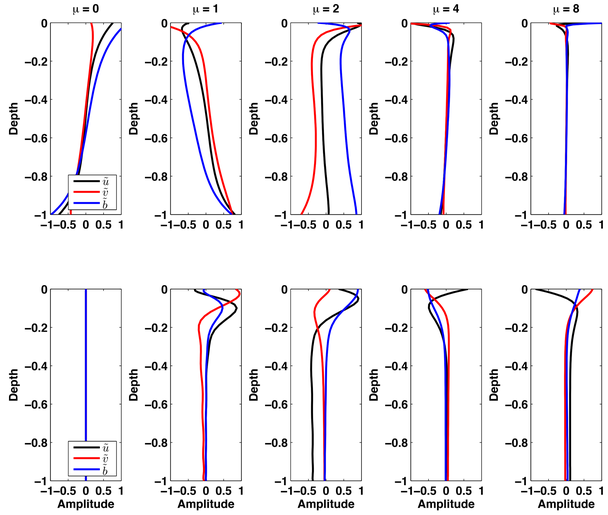

Figure 4. Vertical structure of the perturbation u', v', and b' corresponding to the growth rates shown in Fig. 3. The upper row corresponds to the geostrophic mode, and the lower row corresponds to the wave mode.

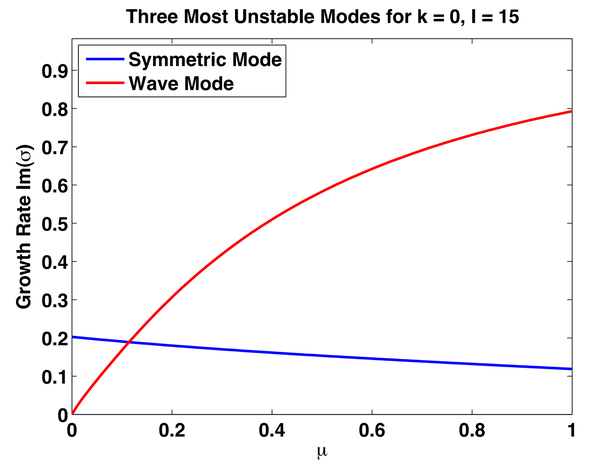

Figure 5. Growth rates vs μ for the two most unstable modes for k = 0, l = 15, Ri = 0.9, α = 0.006, Ro = 0.01, θ = π/4.

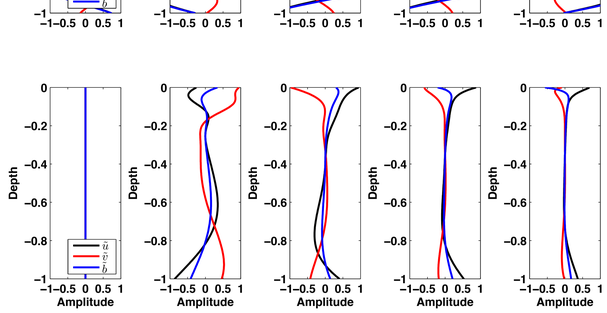

Figure 6. Vertical structure of the perturbation u', v', and b' corresponding to the growth rates shown in Fig. 5. The upper row corresponds to the symmetric mode, and the lower row corresponds to the wave mode.

The vertical structure of each mode shows that the geostrophic mode (fig. 4, upper row) is significantly influenced by the strongly surface intensified Stokes drift, suggesting that the geostrophic mode becomes a mixed mode at modest wave forcing. The wave mode (fig. 4, lower row) shows significant vertical structure near the surface, and very little at depth. This is just what one would expect from a mode generated by the surface intensified Stokes drift. The vertical structure of the wave mode at k = 0, l = 15 is quite different, with significant vertical structure at both the top and bottom.

Conclusions and Future Work

- In the Ro << 1 limit with constant vertical and horizontal stratification, the Lagrangian background flow is unaffected by the wave forcing. The result is thermal wind balance of the Lagrangian flow. The same is not true of general fronts and filaments in the presence of wave forcing (McWilliams and Fox-Kemper, 2012).
- Although the Lagrangian background flow is unaffected by the wave forcing, the O(Ro) perturbation to the O(1) background flow shows significant influence of the Stokes vortex force in the perturbation momentum equations.
- The growth rate shows significant sensitivity to wave forcing and wave direction with high wavenumber instabilities dominating flow with high wave forcing.
- The geostrophic mode is weakly modulated at low wave forcing, and becomes a mixed geostrophic-wave mode at moderate wave forcing.
- The symmetric mode is quickly damped at low wave forcing.
- Future work aims to further characterize the effects of wave forcing on the geostrophic and symmetric instabilities.
- Long term goals include adding a surface wind stress so that the limit of Craik-Leibovich instability can be reached.
- The linear stability results discussed here are intended to guide numerical simulations of the full Boussinesq Craik-Leibovich equations, where the most interesting regions of the Ri, α, Ro, μ, and θ parameter space (as determined by the linear stability analysis) will be examined.

References

- Craik, A. D. D., and Leibovich, S. (1976). A rational model for Langmuir circulations. J. Fluid Mech, 73, 401-426.
- McWilliams, J. C., and Fox-Kemper, B. (2012). Oceanic wave-balanced surface fronts and filaments. J. Fluid Mech, Submitted.
- Stone, P. H. (1971). Baroclinic stability under non-hydrostatic conditions. J. Fluid Mech, 45, 659-671.